Collective spin mode in a multicomponent system of coupled itinerant and localized electrons

Fan Yang,[1] Su-Peng Kou,[2] and Zheng-Yu Weng[3,*]
[1]*Department of Physics, Beijing Institute of Technology, Beijing 100081, People's Republic of China*
[2]*Department of Physics, Beijing Normal University, Beijing 100875, People's Republic of China*
[3]*Institute for Advanced Study, Tsinghua University, Beijing 100084, People's Republic of China*
(Received 26 April 2010; revised manuscript received 12 June 2010; published 29 June 2010)

We study collective spin excitations of a magnetically ordered state in a multicomponent system composed of both itinerant electrons and local moments. Here the induced spin-density-wave (SDW) ordering of itinerant electrons and the collinear antiferromagnetic ordering of local moments are locked together via a Hund's rule coupling. We show that the Goldstone theorem still holds at the random-phase approximation level with the gapless spin wave protected inside the small SDW gap of itinerant electrons, which, however, is fragile in the presence of ion anisotropy. A gapped "out-of-phase" spin mode extending over a much wider energy scale above the SDW gap is found to be more robust against the ion anisotropy, which is mainly contributed by the local moment fluctuations. While the scattering between the Goldstone mode and itinerant electrons diminishes within the SDW gap, the out-of-phase mode will strongly interact with itinerant electrons and thus dominate the spin and charge dynamics in such an ordered phase. Possible relevance of such a model to the iron pnictides will be also discussed.

DOI: 10.1103/PhysRevB.81.245130 PACS number(s): 74.20.Mn, 71.27.+a, 75.20.Hr

I. INTRODUCTION

The recent discovery of high-T_c superconductors in the iron pnictides[1] has renewed a tremendous interest in the interplay between the magnetism and superconductivity. The similar issue has been vigorously investigated in the high-T_c cuprates over two decades, where antiferromagnetism has been firmly related to the localized electrons of the Mott insulator in undoped cuprate compounds.[2] By contrast, in the pnictides, the undoped parent material is not a simple Mott-Hubbard insulator but resembles a multiband bad metal, i.e., the iron 3*d* electrons are believed to be quite itinerant with their hybridized multiorbitals forming multiple Fermi pockets at the Fermi level.[3–7]

It is natural for many to consider the spin-density-wave (SDW) order, observed in the undoped parent compounds by the neutron-scattering measurements,[8] as originated from the same itinerant electrons via Fermi-surface nesting.[3] This picture seems more consistent in explaining the angle-resolved photoemission spectroscopy (ARPES),[9–11] transport,[1,12] and optical properties[13] than a purely localized model, e.g., the J_1-J_2 model,[14–17] where a Mott-insulator transition has been implied. However, a purely itinerant picture is not satisfactory even according to the first-principles calculation. It has been pointed out that local-density approximation is not stable against formation of small moments in Refs. 18–21. This fact suggests that, in density-functional theory and fluctuation exchange approximation approaches, the system does not have strong instability toward stripe antiferromagnetic (AF) order due to the Fermi-surface nesting.[22] On the other hand, a purely localized model is more reasonable in explaining the spin excitations in neutron scattering[17] and high-temperature magnetic susceptibility[23–25] but obviously fails in understanding the bad metal behavior[1,13,26,27] and the presence of the small Fermi pockets[9–11,28,29] in the parent compounds.

Based on the overall experimental evidence, an alternative picture has been recently proposed,[30] which assumes that some kind of orbital-selective Mott transition happens in the iron 3*d* orbitals of the pnictides such that both itinerant and Mott-localized electron coexist in the system. The minimal model[30] based on this picture tries to reconcile the seemingly contradictory experimental facts and provides a natural understanding of the unified driving force behind the collinear AF order and high-temperature superconductivity. Recently a microscopic realization of an orbital-selective Mott transition in the pnictides has been studied[31,32] based on the dynamic mean-field theory, which lends further support to this model.

The key and unique feature for such a coexistent itinerant and localized electron system is that the two subsystems share the *same* characteristic momenta at $\mathbf{Q}_s=(\pi,0)$ or $(0,\pi)$. Namely, the hole and electron Fermi-surface pockets around Γ and M points in the Brillouin zone (BZ) are approximately connected by $\mathbf{Q}_s$ in the undoped case (i.e., close to the Fermi-surface nesting), and at the same time, the local moments are strongly correlated at the AF wave vectors $\mathbf{Q}_s$. As a consequence, the local Hund's rule coupling between the itinerant electrons and local moments can be significantly enhanced around $\mathbf{Q}_s$, which is called the "*resonant effect*."[30] At low temperature, such a resonant effect can serve as a predominant force in driving the *magnetic* or *pairing instability* at different dopings. Here the magnetic phase is predicted[30] to be an induced SDW order of the itinerant electrons locking with the collinear AF order of the local moments at the same $\mathbf{Q}_s$. Corresponding to such an AF ordering, a small SDW gap will open up in the excitation spectrum of itinerant electrons, although *not* necessarily pinned at the Fermi level as in an SDW state purely driven by Fermi-surface nesting. At the mean-field level, the low-lying AF fluctuation of the local moments is also gapped at $\mathbf{Q}_s$ due to the mutual locking of the magnetic orders in the two subsystems. Therefore, after the spontaneous magnetic symmetry breaking, the strong "resonant" scattering between the two degrees of freedom gets substantially reduced, which leads to a very coherent charge transport contributed by the

 ©2010 The American Physical Society

ungapped part of the Fermi surfaces in consistency with the optical measurement.[13]

However, it remains an important issue whether a gapless spin wave, i.e., a Goldstone mode, is still present in the magnetically ordered state of such a multicomponent system. To answer this question, one has to go beyond the mean-field theory to study the collective spin fluctuations, which is also important in order to self-consistently address the issue how the charge dynamics gets reshaped in the AF phase. In this paper, we shall address this issue with using a realistic five-band model[7] to characterize the itinerant electrons near the Fermi pockets, and a J_1-J_2 type model to describe the Mott-localized electrons. Then we study the Hund's rule coupling between the itinerant and localized electrons at the random-phase approximation (RPA) level in the magnetic ordered phase. We demonstrate that the Goldstone theorem indeed holds at the RPA level as a gapless spin wave emerges within the mean-field SDW gap of itinerant electrons. But it is fragile against the ion anisotropy. We further find that the coupling between the Goldstone mode and the charge carriers diminishes in the long wavelength around $\mathbf{Q}_s$ as expected. On the other hand, distinct from a single component system, a gapped "out-of-phase" collective spin mode is also present with its high-energy part predominantly contributed by the local moments whose energy scale $\sim J_2$ extends over a much wider regime than the SDW gap. Its low-energy part gets strongly renormalized by coupling to the itinerant electrons around $\mathbf{Q}_s$—it becomes gapped once the mean-field SDW order forms by itinerant electrons, which is not significantly modified at the RPA level. Furthermore, such an out-of-phase mode is not sensitive to a weak ion-anisotropy effect and is thus more robust than the Goldstone mode. The existence of the two branches of spin excitations in the AF state is a unique prediction of the present multicomponent model. In particular, it is this out-of-phase spin mode that remains strongly interacting with itinerant electrons, at an energy higher than its gap, and therefore dominates the high-energy magnetic and transport properties in the magnetically ordered phase.

The remainder of the paper is organized as follows. In Sec. II, we introduce the model and present the mean-field treatment in the magnetically ordered state. Then in Sec. III, we discuss the spin dynamics at the RPA level and demonstrate that the spin collective excitations are split into a gapless Goldstone mode which is upper-bounded and a gapped out-of-phase mode which extends over a much wider energy scale. In Sec. IV, we study the scattering between the collective spin modes and the itinerant electrons based on the single-particle self-energy of the itinerant electrons and the optical conductivity, which illustrate that the out-of-phase mode will play a dominant role beyond its energy gap. Finally, Sec. V is devoted to the discussion and conclusion.

II. A MULTICOMPONENT SYSTEM OF COUPLED ITINERANT AND LOCALIZED ELECTRONS

A. Model

We consider a multicomponent system composed of coexistent multiband itinerant and Mott-localized electrons described by

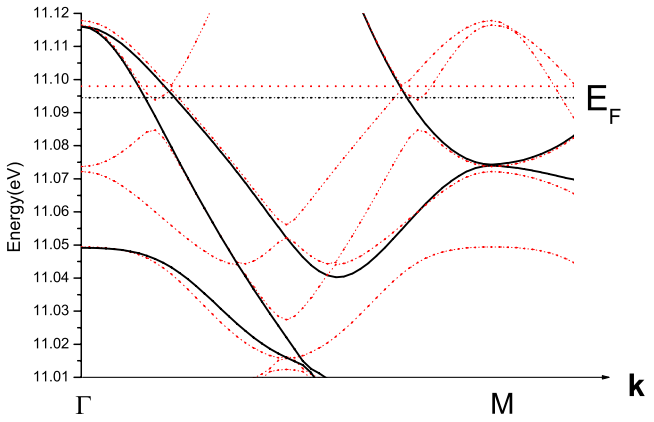

FIG. 1. (Color online) The band structure near the Fermi energy for the five-band model described by $H_{\rm it}$ in Eq. (2) (black solid curves) in the undoped case. The reconstruction of the band structure of itinerant electrons in the presence of a collinear AF order is shown by red dotted curves.

$$H = H_{\rm it} + H_{\rm lo} + H_{J_H}. \tag{1}$$

Here $H_{\rm it}$ is a tight-binding model of multiband itinerant electrons,

$$H_{\rm it} = -\sum_{i,j,m,n,\sigma} t_{ij,mn} c^{\dagger}_{im\sigma} c_{jn\sigma}, \tag{2}$$

where m and n are the orbital indices. The hopping integral $t_{ij,mn}$ in $H_{\rm it}$ will be given based on a realistic five-band tight-binding model proposed[7] to describe the undoped iron-pnictide materials. The resulting band structure near the Fermi energy is shown in Fig. 1 by the solid (black) curves with the Fermi surface shown in Fig. 2(a) in the undoped case (i.e., six electrons per site). Note that some slight modification with a global renormalization factor reducing the bandwidth has been phenomenologically made here in order to be consistent with ARPES.[9–11,29] As shown in Fig. 2(a), the itinerant electrons form hole and electron pockets at the Fermi energy, which are located at the Γ point and the M

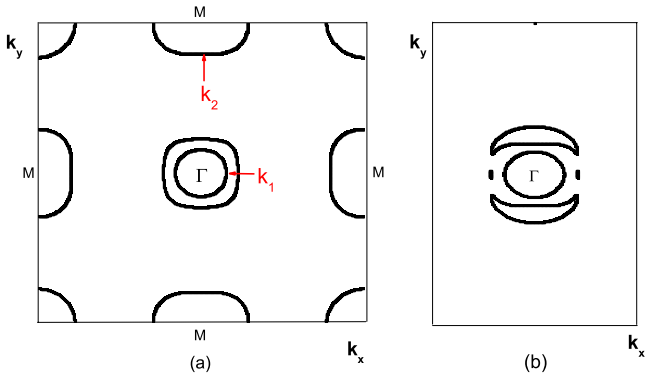

FIG. 2. (Color online) (a) The Fermi pockets of the itinerant electrons in the undoped case. (b) The reconstruction of the Fermi surface in the presence of a collinear AF order with a wave vector $\mathbf{Q}_s=(\pi,0)$ in the reduced BZ.

point, respectively, separated by the momenta $\mathbf{Q}_s$ in an extended BZ.

The second term $H_{\rm lo}$ in Eq. (1) describes the localized electrons in which a Mott gap is opened up via the so-called orbital-selective Mott transition.[30] Namely, the corresponding electrons only contribute to spin fluctuations, near the Fermi energy, by the local moments formed from the filled lower Hubbard band. Note that a microscopic realization of the orbital-selective Mott transition in such a system has been recently discussed based on the dynamic mean-field theory.[31,32] We shall simply use a J_1-J_2 model of $S=1$ to depict the superexchange couplings between these local moments, i.e.,

$$H_{\rm lo} = J_1 \sum_{\langle ij\rangle} \hat{\mathbf{S}}_i \cdot \hat{\mathbf{S}}_j + J_2 \sum_{\langle\langle ij\rangle\rangle} \hat{\mathbf{S}}_i \cdot \hat{\mathbf{S}}_j, \tag{3}$$

where $\langle ij\rangle$ and $\langle\langle ij\rangle\rangle$ denote the nearest-neighbor and next-nearest-neighbor coupling, respectively. Here we assume $J_1 < 2J_2$ such that the ground state of $H_{\rm lo}$ itself may form a collinear AF ordering at the wave vector $\mathbf{Q}_s$. In principle, the same five-band electrons in iron pnictides should contribute to both itinerant and local moment degrees of freedom. But for simplicity we treat $H_{\rm it}$ and $H_{\rm lo}$ as if they govern *independent* degrees of freedom in the low-energy sector near the Fermi energy, as long as the Mott gap remains a large energy scale. We ignore the issues like how the Fermi-surface shape gets affected by the orbital-selective Mott transition as well as how the Luttinger volume is correctly accounted for and mainly focus on the low-energy physics in the present work.

The third term H_{J_H} in Eq. (1) is the Hund's rule coupling between the spins of itinerant and the localized electrons,

$$H_{J_H} = -\sum_{i,m} J_0^m \hat{\mathbf{S}}_i \cdot \hat{\mathbf{s}}_{im}, \tag{4}$$

where $\hat{\mathbf{s}}_{im} = c_{im}^\dagger \hat{\sigma} c_{im}$ is the spin operator of the itinerant electrons in the mth orbital and $\hat{\mathbf{S}}_i$ denotes the localized moment at site i. J_0^m is a renormalized Hund's rule coupling constant. For simplicity, we shall assume a single $J_0^m = J_0$ for different orbitals throughout the paper.

Originally a simpler form of Eq. (1) was proposed as a minimal model to describe the low-energy physics in the iron pnictides.[30] The most important feature in such a model Hamiltonian is that the peculiar momenta $\mathbf{Q}_s$, which on the one hand connects the two Fermi pockets of the itinerant electrons at Γ and M points, respectively, and on the other hand coincide with the AF wave vectors of the local moments. It implies *strongly enhanced* dynamic coupling between the itinerant and local moment degrees of freedom, once the short-range AF correlations of the local moments set in around $\mathbf{Q}_s$ even in a high-temperature normal state. With the decrease of temperature, such a resonant coupling will result in an AF ordered phase with distinctive dynamic behaviors to be explored below, as compared to an ordinary SDW state of a pure itinerant electron system due to the Fermi-surface nesting mechanism or the collinear AF state of a pure J_1-J_2 mode.

B. Mean-field treatment in the collinear AF ordered state

In the following we first use a mean-field approximation to study the collinear AF ordered state in Eq. (1). The spin and charge dynamics at the RPA level will be investigated in the later sections.

We start with the interaction term H_{J_H} in Eq. (4) between the two subsystems. By introducing two order parameters of magnetization for the local moments, $M_{\rm (lo)}$, and itinerant electrons, $M_{\rm (it)}$, respectively, as in $\langle \hat{S}_i^z \rangle \equiv M_{\rm (lo)} e^{i\mathbf{Q}_s\cdot\mathbf{r}_i}$ and $\Sigma_m \langle \hat{s}_{im}^z \rangle \equiv M_{\rm (it)} e^{i\mathbf{Q}_s\cdot\mathbf{r}_i}$, one obtains the following linearization in H_{J_H}, given by

$$H_{J_H} \to H_I = -J_0 \sum_i \left[M_{\rm (lo)} e^{i\mathbf{Q}_s\cdot\mathbf{r}_i} \sum_m s_{im}^z + M_{\rm (it)} e^{i\mathbf{Q}_s\cdot\mathbf{r}_i} \hat{S}_i^z \right] \equiv H_{I\rm (it)} + H_{I\rm (lo)}. \tag{5}$$

Below the effect of such mean-field terms on the local moments and itinerant electrons will be explored in a self-consistent way.

1. Local-moment part

In the magnetic order phase with $\langle \hat{S}_i^z \rangle = M_{\rm (lo)} e^{i\mathbf{Q}_s\cdot\mathbf{r}_i}$, one may first use the conventional spin-wave approximation to treat $H_{\rm lo}$ in Eq. (3) and then add $H_{I\rm (lo)}$ in Eq. (5) to incorporate the effect of the coupling to the itinerant electrons. Here $\mathbf{Q}_s$ is chosen to be $(\pi,0)$.

Introduce the Holstein-Primakoff (HP) transformation,

$$\hat{S}_{iA}^+ = \sqrt{2S - a_i^\dagger a_i}\, a_i, \quad \hat{S}_{iA}^- = a_i^\dagger \sqrt{2S - a_i^\dagger a_i}, \quad \hat{S}_{iA}^z = S - a_i^\dagger a_i,$$

$$\hat{S}_{jB}^+ = \sqrt{2S - b_j^\dagger b_j}\, b_j^\dagger, \quad \hat{S}_{jB}^- = b_j \sqrt{2S - b_j^\dagger b_j}, \quad \hat{S}_{jB}^z = -S + b_j^\dagger b_j, \tag{6}$$

where A and B sublattices are defined by the staggered factor $e^{i\mathbf{Q}_s\cdot\mathbf{r}_i} = \pm 1$. Under the approximation $\sqrt{2S - a_i^\dagger a_i} \approx \sqrt{2S - b_i^\dagger b_i} \approx \sqrt{2S}$ and using the boson operators in the momentum space,

$$a_i = \left(\frac{2}{N}\right)^{1/2} {\sum_{\mathbf{k}}}' a_{\mathbf{k}} \exp(i\mathbf{k}\cdot\mathbf{r}_i), \tag{7}$$

$$b_j = \left(\frac{2}{N}\right)^{1/2} {\sum_{\mathbf{k}}}' b_{\mathbf{k}} \exp(i\mathbf{k}\cdot\mathbf{r}_j), \tag{8}$$

$H_{\rm lo}$ is transformed into

$$H_{\rm lo} = S {\sum_{\mathbf{k}}}' [\Gamma_{\mathbf{k}} (a_{\mathbf{k}}^\dagger a_{\mathbf{k}} + b_{\mathbf{k}}^\dagger b_{\mathbf{k}}) + M_{\mathbf{k}} (a_{\mathbf{k}} b_{-\mathbf{k}} + a_{\mathbf{k}}^\dagger b_{-\mathbf{k}}^\dagger)], \tag{9}$$

where $\Sigma_{\mathbf{k}}'$ means that the sum is within a reduced BZ with

$$\Gamma_{\mathbf{k}} = 4J_2 + 2J_1 \cos k_y, \tag{10}$$

$$M_{\mathbf{k}} = 2J_1 \cos k_x + 4J_2 \cos k_x \cdot \cos k_y. \tag{11}$$

Then Eq. (9) can be diagonalized by the Bogolubov transformation,

$$a_{\mathbf{k}} = u_{\mathbf{k}}\alpha_k + v_{\mathbf{k}}\beta^{\dagger}_{-\mathbf{k}},$$

$$b^{+}_{-\mathbf{k}} = v_{\mathbf{k}}\alpha_k + u_{\mathbf{k}}\beta^{\dagger}_{-\mathbf{k}}, \tag{12}$$

as follows:

$$H_{\mathrm{lo}} = \sum_{\mathbf{k}}{}' \omega_{\mathbf{k}}(\alpha^{\dagger}_{\mathbf{k}}\alpha_{\mathbf{k}} + \beta^{\dagger}_{\mathbf{k}}\beta_{\mathbf{k}}), \tag{13}$$

where

$$u_{\mathbf{k}} = \left(\frac{\omega_{\mathbf{k}} + \Gamma_{\mathbf{k}}}{2\omega_{\mathbf{k}}}\right)^{1/2}, \tag{14}$$

$$v_{\mathbf{k}} = -\left(\frac{-\omega_{\mathbf{k}} + \Gamma_{\mathbf{k}}}{2\omega_{\mathbf{k}}}\right)^{1/2} \mathrm{sgn}(M_{\mathbf{k}}), \tag{15}$$

$$\omega_{\mathbf{k}} = S\sqrt{\Gamma^2_{\mathbf{k}} - M^2_{\mathbf{k}}}. \tag{16}$$

Here $\omega_{\mathbf{k}}$ is gapless at $\mathbf{k}=\mathbf{Q}_s$ as the Goldstone mode of H_{lo} in the AF ordered phase.

Now let us add $H_{I(\mathrm{lo})}$ in Eq. (5) arising from the mean-field decoupling of H_{J_H}. It can be re-expressed in the spin-wave formalism by

$$H_{I(\mathrm{lo})} = J_0 M_{(\mathrm{it})} \sum_{\mathbf{k}}{}' (a^{\dagger}_{\mathbf{k}}a_{\mathbf{k}} + b^{\dagger}_{\mathbf{k}}b_{\mathbf{k}}) + \mathrm{const.} \tag{17}$$

This term will lead to a shift in $\Gamma_{\mathbf{k}}$ defined in Eq. (10): i.e., $\Gamma_{\mathbf{k}} \to \Gamma_{\mathbf{k}} + J_0 M_{(\mathrm{it})}/S$. As a result, the dispersion of the spin wave is modified by

$$\omega_{\mathbf{k}} \to \omega_{\mathbf{k}} = S\sqrt{(\Gamma_{\mathbf{k}} + J_0 M_{(\mathrm{it})}/S)^2 - M^2_{\mathbf{k}}}. \tag{18}$$

In particular, $\omega_{\mathbf{k}}$ is no longer gapless at $\mathbf{Q}_s$ with an energy gap induced by $M_{(\mathrm{it})}$ as

$$\omega_{\mathbf{Q}_s} = \sqrt{4M_{(\mathrm{it})}SJ_0(2J_2 + J_1) + (M_{(\mathrm{it})}J_0)^2}. \tag{19}$$

The order parameter $M_{(\mathrm{lo})}$ can be self-consistently calculated as

$$M_{(\mathrm{lo})} = S - \frac{1}{N}\left\langle \sum_{\mathbf{k}}{}' (a^{\dagger}_{\mathbf{k}}a_{\mathbf{k}} + b^{\dagger}_{\mathbf{k}}b_{\mathbf{k}}) \right\rangle = S - \frac{2}{N}\sum_{\mathbf{k}}{}' v^2_{\mathbf{k}}, \tag{20}$$

where $v_{\mathbf{k}}$ is defined by Eq. (15) with $\Gamma_{\mathbf{k}} \to \Gamma_{\mathbf{k}} + J_0 M_{(\mathrm{it})}/S$ and $\omega_{\mathbf{k}}$ defined in Eq. (18).

Finally, the spin-spin correlations for the local moment defined by

$$\chi^{+-}_{(\mathrm{lo})}(\mathbf{q},\mathbf{q},t) = -i\langle T\hat{S}^{+}_{\mathbf{q}}(t)\hat{S}^{-}_{-\mathbf{q}}(0)\rangle,$$

$$\chi^{+-}_{(\mathrm{lo})}(\mathbf{q},\mathbf{q}+\mathbf{Q}_s,t) = -i\langle T\hat{S}^{+}_{\mathbf{q}}(t)\hat{S}^{-}_{-\mathbf{q}-\mathbf{Q}_s}(0)\rangle$$

can be obtained for this mean-field spin-wave state in the frequency space as

$$\chi^{+-}_{(\mathrm{lo})0}(\mathbf{q},\mathbf{q},\omega) = M_{(\mathrm{lo})}(u_{\mathbf{k}} + v_{\mathbf{k}})^2 \times\left(\frac{1}{\omega - \omega_{\mathbf{k}} + i0^+} + \frac{1}{-\omega - \omega_{\mathbf{k}} + i0^+}\right),$$

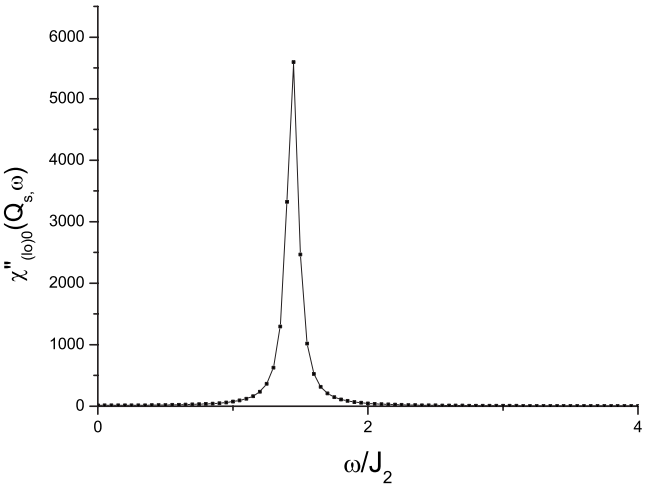

FIG. 3. Dynamic spin susceptibility of local moments at mean-field level, i.e., $\chi''_{(\mathrm{lo})0\mathbf{q}}(\omega) \equiv -2\ \mathrm{Im}\ \chi^{+-}_{(\mathrm{lo})0}(\mathbf{q},\mathbf{q},\omega)$ at $\mathbf{q}=\mathbf{Q}_s$ shows a gap, given by Eq. (19), which is opened up in the presence of a mean-field coupling to the SDW ordering of itinerant electrons, with the parameters given in Sec. II B.

$$\chi^{+-}_{(\mathrm{lo})0}(\mathbf{q},\mathbf{q}+\mathbf{Q}_s,\omega) = M_{(\mathrm{lo})}\left(\frac{1}{\omega - \omega_{\mathbf{k}} + i0^+} - \frac{1}{-\omega - \omega_{\mathbf{k}} + i0^+}\right). \tag{21}$$

The spin gap in Eq. (19) is clearly illustrated in the dynamic spin susceptibility $\chi''_{(\mathrm{lo})0\mathbf{q}}(\omega) \equiv -2\ \mathrm{Im}\ \chi^{+-}_{(\mathrm{lo})0}(\mathbf{q},\mathbf{q},\omega)$ at $\mathbf{q}=\mathbf{Q}_s$ as shown in Fig. 3 (the parameters used are to be given below). It is pointed out that in the above calculation, we have further used the approximation: $S^{+}_{iA(B)} \to \sqrt{2M_{(\mathrm{lo})}}a^{\dagger}_i(\sqrt{2M_{(\mathrm{lo})}}b^{\dagger}_i)$ in the original HP transformation, Eq. (6), such that the spin commutation relations are satisfied at the mean-field level, i.e., $\langle\hat{\mathbf{S}}\times\hat{\mathbf{S}}\rangle = i\hbar\langle\hat{\mathbf{S}}\rangle$.

2. Itinerant electron part

Combining $H_{I(\mathrm{it})}$ in Eq. (5) with the band kinetics energy term H_{it} in Eq. (2), the mean-field Hamiltonian of the itinerant electrons reads

$$\begin{aligned} H_{\mathrm{it}} + H_{I(\mathrm{it})} &= \sum_{\mathbf{k}mn\sigma}{}' \left[f_{mn}(\mathbf{k}) c^{+}_{\mathbf{k}m\sigma}c_{\mathbf{k}n\sigma} + f_{mn}(\mathbf{k}+\mathbf{Q}_s)c^{\dagger}_{\mathbf{k}+\mathbf{Q}_s,m\sigma}c_{\mathbf{k}+\mathbf{Q}_s,n\sigma} \right. \\ &\quad \left. - \frac{J_0 M_{(\mathrm{lo})}\sigma}{2}\delta_{mn}(c^{\dagger}_{\mathbf{k}+\mathbf{Q}_s,m\sigma}c_{\mathbf{k},n\sigma} + c^{\dagger}_{\mathbf{k},m\sigma}c_{\mathbf{k}+\mathbf{Q}_s,n\sigma}) \right] \\ &\equiv \sum_{\mathbf{k}\sigma}{}' X^{\dagger}_{\mathbf{k}\sigma}H_{\sigma}X_{\mathbf{k}\sigma}, \end{aligned} \tag{22}$$

where

$$f_{mn}(\mathbf{k}) = 2\sum_{\mathbf{r}_i - \mathbf{r}_j} t_{ij,mn}e^{i\mathbf{k}\cdot(\mathbf{r}_i - \mathbf{r}_j)}. \tag{23}$$

2In the second line of Eq. (22), the 10×10 matrix H_σ for the five bands is defined by

$$(H)_\sigma = \begin{pmatrix} F_{\mathbf{k}} & -\gamma I\sigma \\ -\gamma I\sigma & F_{\mathbf{k}+\mathbf{Q}_s} \end{pmatrix} \tag{24}$$

with

$$\gamma = \frac{J_0 M_{(\mathrm{lo})}}{2}. \tag{25}$$

Here I is the 5×5 identity matrix and F is the matrix defined by $(F)_{m,n}=f_{mn}$. The column vector $X_{\mathbf{k}\sigma}$ is given by

$$X^T_{\mathbf{k}\sigma} \equiv (c_{\mathbf{k},1\sigma}, c_{\mathbf{k},2\sigma}, \ldots, c_{\mathbf{k}+\mathbf{Q}_s,1\sigma} c_{\mathbf{k}+\mathbf{Q}_s,2\sigma}, \ldots). \tag{26}$$

By diagonalizing the 10×10 matrix $(H)_\sigma$,

$$U^\dagger_\sigma H_\sigma U_\sigma = D, \tag{27}$$

one gets

$$H_{\mathrm{it}} + H_{I(\mathrm{it})} = {\sum_{\mathbf{k}\alpha\sigma}}' E_{\mathbf{k}\alpha} c^\dagger_{\mathbf{k}\alpha\sigma} c_{\mathbf{k}\alpha\sigma}, \tag{28}$$

where the band energy $E_{\mathbf{k}\alpha}$ is equal to the αth diagonal element of D, presented in Fig. 1 by the red dotted curves with the corresponding Fermi surface in the reduced BZ shown in Fig. 2(b) in the undoped case. Here the order parameter $M_{(\mathrm{it})}$ is self-consistently determined by

$$\begin{aligned} M_{(\mathrm{it})} &= \frac{1}{2N}\sum_{in} e^{i\mathbf{Q}_s\cdot\mathbf{r}_i}\langle c^\dagger_{in\uparrow} c_{in\uparrow} - c^\dagger_{in\downarrow} c_{in\downarrow}\rangle \\ &= \frac{2}{N}{\sum_{E_{\mathbf{k}\alpha}<E_F}}' \sum_n U^*_{\mathbf{k}\uparrow}(n+5,\alpha) U_{\mathbf{k}\uparrow}(n,\alpha). \end{aligned} \tag{29}$$

Together with Eq. (20), we find $M_{(\mathrm{it})}=0.252$ and $M_{(\mathrm{lo})}=0.892$ by choosing $J_0=20$ meV at $J_1=0$ and $J_2=20$ meV for $S=1$. In the following we shall use these parameters to examine various spin and charge dynamics (we have also checked other small ratios of J_1/J_2 and found the results remain qualitatively unchanged).

Similar mean-field results have been previously obtained[30] in a simpler model of Eq. (1), where a spin gap similar to Eq. (19) is also found in the spin-wave spectrum of local moments due to the Hund's rule coupling to the SDW order of the itinerant electrons. Such a gap will protect the collinear AF ordering jointly formed by *both* local moments and itinerant electrons below a transition temperature T_{SDW}. For example, the presence of this gap is reflected by a steep reduction in the uniform spin susceptibility below T_{SDW}, which is consistent[30] with the experimental measurement in the iron pnictides.[23,24] However, according to the Goldstone theorem, a gapless mode is generally expected to exist in the AF ordered state. How such a Goldstone mode can be reconciled with the gapped local moment fluctuations discussed above will be studied at the RPA level in the next section.

Finally, the spin-spin correlation functions of itinerant electrons are defined as

$$\chi^{+-}_{(\mathrm{it})}(\mathbf{q},\mathbf{q},t) = -i\langle T\hat{s}^+_{\mathbf{q}}(t)\hat{s}^-_{-\mathbf{q}}(0)\rangle,$$

$$\chi^{+-}_{(\mathrm{it})}(\mathbf{q},\mathbf{q}+\mathbf{Q}_s,t) = -i\langle T\hat{s}^+_{\mathbf{q}}(t)\hat{s}^-_{-\mathbf{q}-\mathbf{Q}_s}(0)\rangle,$$

where $\hat{s}^\pm_{\mathbf{q}}$ is the sum over all the five orbital

$$\hat{s}^\pm_{\mathbf{q}} = \sum_m \hat{s}^\pm_{\mathbf{q}m}. \tag{30}$$

In the above mean-field state, after a straightforward but tedious calculation one obtains, for example,

$$\begin{aligned} \chi^{+-}_{(\mathrm{it})0}(\mathbf{q},\mathbf{q},\omega) = &\sum_{\mathbf{k}\in R,\mathbf{k}+\mathbf{q}\in R,E_{\mathbf{k},\alpha}>E_F,E_{\mathbf{k}+\mathbf{q},\beta}<E_F} \frac{|V^{(1)}_{\mathbf{k},\mathbf{k}+\mathbf{q}}(\alpha,\beta)|^2}{\omega-(E_{\mathbf{k},\alpha}-E_{\mathbf{k}+\mathbf{q},\beta})+i0^+} + \sum_{\mathbf{k}\in R,\mathbf{k}+\mathbf{q}\notin R,E_{\mathbf{k},\alpha}>E_F,E_{\mathbf{k}+\mathbf{q}\pm\mathbf{Q}_s,\beta}<E_F} \frac{|V^{(2)}_{\mathbf{k},\mathbf{k}+\mathbf{q}\pm\mathbf{Q}_s}(\alpha,\beta)|^2}{\omega-(E_{\mathbf{k},\alpha}-E_{\mathbf{k}+\mathbf{q}\pm\mathbf{Q}_s,\beta})+i0^+} \\ &+ \sum_{\mathbf{k}\in R,\mathbf{k}-\mathbf{q}\in R,E_{\mathbf{k},\alpha}>E_F,E_{\mathbf{k}-\mathbf{q},\beta}<E_F} \frac{|V^{(1)}_{\mathbf{k}-\mathbf{q},\mathbf{k}}(\beta,\alpha)|^2}{-\omega-(E_{\mathbf{k},\alpha}-E_{\mathbf{k}-\mathbf{q},\beta})+i0^+} \\ &+ \sum_{\mathbf{k}\in R,\mathbf{k}-\mathbf{q}\notin R,E_{\mathbf{k},\alpha}>E_F,E_{\mathbf{k}-\mathbf{q}\pm\mathbf{Q}_s,\beta}<E_F} \frac{|V^{(2)}_{\mathbf{k}-\mathbf{q}\pm\mathbf{Q}_s,\mathbf{k}}(\beta,\alpha)|^2}{-\omega-(E_{\mathbf{k},\alpha}-E_{\mathbf{k}-\mathbf{q}\pm\mathbf{Q}_s,\beta})+i0^+}, \end{aligned} \tag{31}$$

for the momentum $\mathbf{q}$ within the reduced BZ, i.e., $\mathbf{q}\in R$, and

$$\begin{aligned} V^{(1)}_{\mathbf{k},\mathbf{q}}(\alpha,\beta) \equiv \sum_m [&U^*_{\mathbf{k}\downarrow}(m,\alpha) U_{\mathbf{q}\uparrow}(m,\beta) \\ &+ U^*_{\mathbf{k}\downarrow}(m+5,\alpha) U_{\mathbf{q}\uparrow}(m+5,\beta)], \end{aligned}$$

$$\begin{aligned} V^{(2)}_{\mathbf{k},\mathbf{q}}(\alpha,\beta) \equiv \sum_m [&U^*_{\mathbf{k}\downarrow}(m,\alpha) U_{\mathbf{q}\uparrow}(m+5,\beta) \\ &+ U^*_{\mathbf{k}\downarrow}(m+5,\alpha) U_{\mathbf{q}\uparrow}(m,\beta)] \end{aligned} \tag{32}$$

with, say,

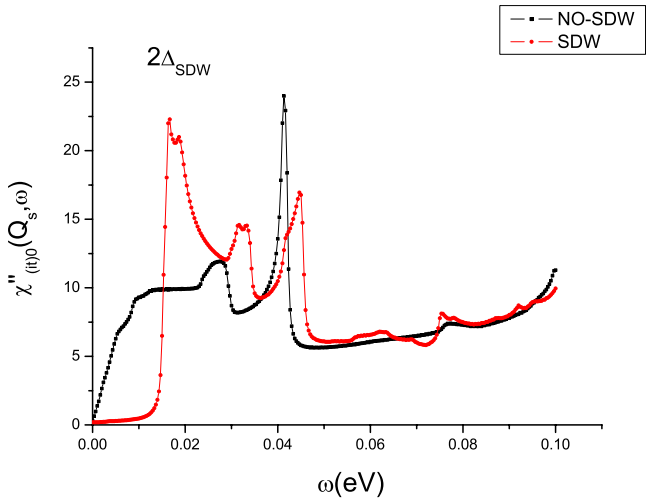

FIG. 4. (Color online) Dynamic spin susceptibility of itinerant electrons at the mean-field level, i.e., $\chi''_{(it)0\mathbf{Q}_s}(\omega) \equiv -2\ \mathrm{Im}\ \chi^{+-}_{(it)0}(\mathbf{Q}_s,\mathbf{Q}_s,\omega)$ with and without SDW order. A gap $2\Delta_{SDW}$ in the SDW ordered case is clearly shown.

$$\hat{s}^-_{-\mathbf{q}} = \sum_{\alpha\beta,\mathbf{k}\in R,\mathbf{k}+\mathbf{q}\in R} c^\dagger_{\mathbf{k},\alpha,\downarrow} c_{\mathbf{k}+\mathbf{q},\beta\uparrow} V^{(1)}_{\mathbf{k},\mathbf{k}+\mathbf{q}}(\alpha,\beta) + \sum_{\alpha\beta,\mathbf{k}\in R,\mathbf{k}+\mathbf{q}\notin R} c^\dagger_{\mathbf{k},\alpha,\downarrow} c_{\mathbf{k}+\mathbf{q}\pm\mathbf{Q}_s,\beta\uparrow} V^{(2)}_{\mathbf{k},\mathbf{k}+\mathbf{q}\pm\mathbf{Q}_s}(\alpha,\beta). \tag{33}$$

The other Green's function can be similarly obtained. Numerical calculation for the dynamic spin susceptibility of the itinerant electrons at the mean-field level, i.e., $\chi''_{(it)0\mathbf{Q}_s}(\omega) \equiv -2\ \mathrm{Im}\ \chi^{+-}_{(it)0}(\mathbf{Q}_s,\mathbf{Q}_s,\omega)$ is presented in Fig. 4 with and without SDW order, where the suppressing of the low-frequency spectrum by the SDW gap at $2\Delta_{SDW}$ is clearly shown.

III. SPIN DYNAMICS

In this section, we shall calculate the dynamic spin susceptibility at the RPA level beyond the above mean-field approximation, by which both a Goldstone mode and a gapped collective spin mode in the AF ordered phase can be recovered.

A. RPA treatment

The Hund's rule interaction between the local moments and itinerant electrons in Eq. (4) is rewritten as

$$H_{J_H} = -J_0 \sum_{\mathbf{q}} \hat{\mathbf{S}}_{\mathbf{q}} \cdot \hat{\mathbf{s}}_{-\mathbf{q}}, \tag{34}$$

where the spin operator $\hat{\mathbf{s}}$ appears as a whole for the five band. At the RPA level, for example,

$$\begin{aligned}\chi^{+-}_{(it)}(\mathbf{q},\mathbf{q},t) &= -i\langle T\hat{s}^+_{\mathbf{q}}(t)\hat{s}^-_{-\mathbf{q}}\rangle_0 + \frac{i}{2}\langle T\hat{s}^+_{\mathbf{q}}(t)H_{J_H}(t_1)H_{J_H}(t_2)\hat{s}^-_{-\mathbf{q}}\rangle_0 \\ &+ O(H^4_{J_H}) = \chi^{+-}_{(it)0}(\mathbf{q},\mathbf{q},t) \\ &+ \left(\frac{J_0}{2}\right)^2 \int_{-\infty}^{\infty} dt_1 \int_{-\infty}^{\infty} dt_2 [\chi^{+-}_{(it)0}(\mathbf{q},\mathbf{q},t \\ &- t_1)\chi^{+-}_{(lo)0}(\mathbf{q},\mathbf{q},t_1-t_2)\chi^{+-}_{(it)0}(\mathbf{q},\mathbf{q},t_2) + \chi^{+-}_{(it)0}(\mathbf{q},\mathbf{q},t \\ &- t_1)\chi^{+-}_{(lo)0}(\mathbf{q},\mathbf{q},t_1-t_2)\chi^{+-}_{(it)0}(\mathbf{q}+\mathbf{Q_s},\mathbf{q},t_2) \\ &+ \chi^{+-}_{(it)0}(\mathbf{q},\mathbf{q}+\mathbf{Q_s},t-t_1)\chi^{+-}_{(lo)0}(\mathbf{q}+\mathbf{Q_s},\mathbf{q}+\mathbf{Q_s},t_1 \\ &- t_2)\chi^{+-}_{(it)0}(\mathbf{q}+\mathbf{Q_s},\mathbf{q},t_2) + \chi^{+-}_{(it)0}(\mathbf{q},\mathbf{q}+\mathbf{Q_s},t \\ &- t_1)\chi^{+-}_{(lo)0}(\mathbf{q}+\mathbf{Q_s},\mathbf{q},t_1-t_2)\chi^{+-}_{(it)0}(\mathbf{q},\mathbf{q},t_2)] + \cdots,\end{aligned} \tag{35}$$

which is illustrated diagrammatically by Fig. 5.

To make the formulation more compact, we define a 2×2 matrix $\hat{\chi}^{+-}(\mathbf{q},\omega)$ with the components

$$\hat{\chi}^{+-}_{(1,1)}(\mathbf{q},\omega) \equiv \chi^{+-}(\mathbf{q},\mathbf{q},\omega),$$

$$\hat{\chi}^{+-}_{(1,2)}(\mathbf{q},\omega) \equiv \chi^{+-}(\mathbf{q},\mathbf{q}+\mathbf{Q}_s,\omega),$$

$$\hat{\chi}^{+-}_{(2,2)}(\mathbf{q},\omega) \equiv \chi^{+-}(\mathbf{q}+\mathbf{Q}_s,\mathbf{q}+\mathbf{Q}_s,\omega),$$

$$\hat{\chi}^{+-}_{(2,1)}(\mathbf{q},\omega) \equiv \chi^{+-}(\mathbf{q}+\mathbf{Q}_s,\mathbf{q},\omega). \tag{36}$$

With this definition, the Fourier transformation of Eq. (35) reads

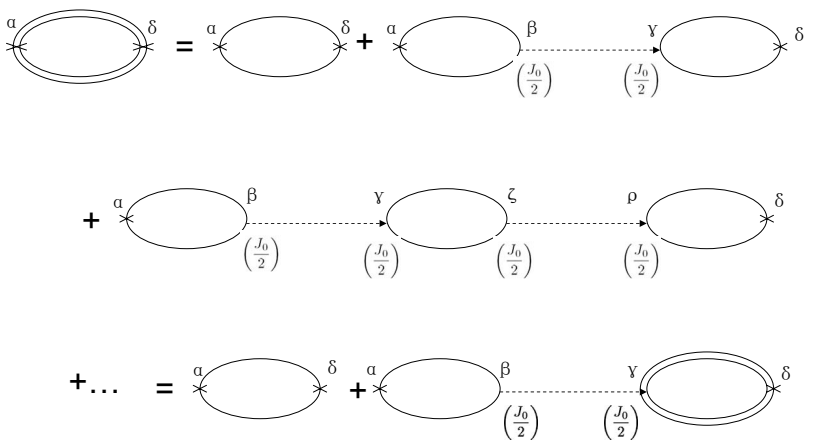

FIG. 5. Feynman diagrams of RPA for dynamic spin correlation of itinerant electrons. Here the single line bubbles denote the dynamic spin correlation function of (free) itinerant electrons, $\hat{\chi}^{+-}_{(it)0}(\mathbf{q},\omega)$, the double line bubbles are the renormalized dynamic spin correlation function of itinerant electrons, $\hat{\chi}^{+-}_{(it)}(\mathbf{q},\omega)$, the dotted lines are the dynamic spin correlation function of local moments, $\hat{\chi}^{+-}_{(lo)0}(\mathbf{q},\omega)$. The indices $\alpha,\beta,\ldots$ label the matrix elements defined in Eq. (36).

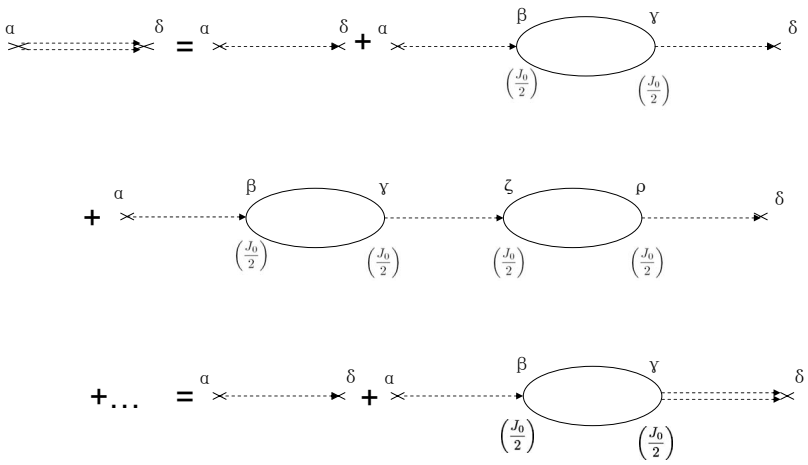

FIG. 6. Feynman diagrams of RPA for dynamic spin correlation of local moments. Here the double dotted lines are the renormalized dynamic spin correlation function of local moments $\hat{\chi}^{+-}_{(\mathrm{lo})}(\mathbf{q},\omega)$. The other symbols are the same as in Fig. 5.

$$\hat{\chi}^{+-}_{(\mathrm{it})(1,1)} = \hat{\chi}^{+-}_{(\mathrm{it})0(1,1)} + \left(\frac{J_0}{2}\right)^2 \sum_{i,j=1,2} \hat{\chi}^{+-}_{(\mathrm{it})0(1,i)} \hat{\chi}^{+-}_{(\mathrm{lo})0(i,j)} \hat{\chi}^{+-}_{(\mathrm{it})0(j,1)} + \cdots, \tag{37}$$

and more generally

$$\hat{\chi}^{+-}_{(\mathrm{it})(i,j)} = \hat{\chi}^{+-}_{(\mathrm{it})0(i,j)} + \left(\frac{J_0}{2}\right)^2 \sum_{i',j'=1,2} \hat{\chi}^{+-}_{(\mathrm{it})0(i,i')} \hat{\chi}^{+-}_{(\mathrm{lo})0(i',j')} \hat{\chi}^{+-}_{(\mathrm{it})0(j',j)} + \cdots. \tag{38}$$

As the Dyson equations in a compact matrix form, the above RPA result for the itinerant electrons can be re-expressed as

$$\hat{\chi}^{+-}_{(\mathrm{it})}(\mathbf{q},\omega) = \left[I - \left(\frac{J_0}{2}\right)^2 \hat{\chi}^{+-}_{(\mathrm{it})0}(\mathbf{q},\omega) \hat{\chi}^{+-}_{(\mathrm{lo})0}(\mathbf{q},\omega) \right]^{-1} \hat{\chi}^{+-}_{(\mathrm{it})0}(\mathbf{q},\omega), \tag{39}$$

and similarly for the local moment part illustrated by Fig. 6, we have

$$\hat{\chi}^{+-}_{(\mathrm{lo})}(\mathbf{q},\omega) = \left[I - \left(\frac{J_0}{2}\right)^2 \hat{\chi}^{+-}_{(\mathrm{lo})0}(\mathbf{q},\omega) \hat{\chi}^{+-}_{(\mathrm{it})0}(\mathbf{q},\omega) \right]^{-1} \hat{\chi}^{+-}_{(\mathrm{lo})0}(\mathbf{q},\omega) \tag{40}$$

with the total dynamic spin susceptibility matrix given by

$$\hat{\chi}^{+-}_{\mathrm{RPA}}(\mathbf{q},\omega) = \hat{\chi}^{+-}_{(\mathrm{it})}(\mathbf{q},\omega) + \hat{\chi}^{+-}_{(\mathrm{lo})}(\mathbf{q},\omega). \tag{41}$$

B. Collective spin modes

Now we focus on the total dynamic spin susceptibility defined by

$$\chi''_{\mathrm{RPA}}(\mathbf{q},\omega) = -2\ \mathrm{Im}\ \hat{\chi}^{+-}_{\mathrm{RPA}(1,1)}(\mathbf{q},\omega) m, \tag{42}$$

which can be numerically determined based on the RPA expressions (39)–(41) given in Sec. III A.

In Fig. 7, $\chi''_{\mathrm{RPA}}(\mathbf{q},\omega)$ at a fixing $\mathbf{q}=\mathbf{Q}_s$ is shown as a function of ω. Here we find a sharp peak emerges at $\omega=0$, in contrast to Figs. 3 and 4. Namely a zero-mode (Goldstone mode) pole is indeed restored at $\mathbf{q}=\mathbf{Q}_s$ in the RPA spin-spin correlation function. Mathematically, it originates from the vanishing denominator in Eqs. (39) and (40).

It is interesting to note that besides the Goldstone mode, there remains a high-energy mode as represented by the hump in Fig. 7. It can be traced to the pole of $\hat{\chi}^{+-}_{(\mathrm{lo})0}(\mathbf{q},\omega)$ (cf. Fig. 3), only broadened through the scattering with the itinerant electrons. In other words, the gapped collective mode of the local moments identified in the mean-field state in the previous section is still present at the RPA level. Physically this gapped mode is an out-of-phase fluctuations of the local moments relative to the magnetization of itinerant electrons while the Goldstone mode is the "in-phase" fluctuations of the locked magnetizations from the local moments and itinerant electrons.

To display the spin dynamics of the system in the whole BZ, the calculated $\chi''_{\mathrm{RPA}}(\mathbf{q},\omega)$ is presented in Fig. 8(a) with the x axis representing the momentum $\mathbf{q}$ along the high-symmetry lines in the reduced BZ and the y axis for the frequency ω, while the brightness depicting the spectral weight $\chi''_{\mathrm{RPA}}(\mathbf{q},\omega)$. From Fig. 8(a), it is clearly shown that the spin excitation spectrum in the AF ordered phase is separated into two branches, i.e., the lower Goldstone-mode branch and the upper out-of-phase mode branch. The dispersions of the two modes are illustrated in Fig. 8(b), which are defined by $(\mathbf{q},\omega)$ at the largest (brightest) $\chi''_{\mathrm{RPA}}(\mathbf{q},\omega)$ in Fig. 8(a). The spin-wave dispersion of the pure J_1-J_2 model, i.e., Eq. (16) and that of the gapped one, Eq. (18), due to cou-

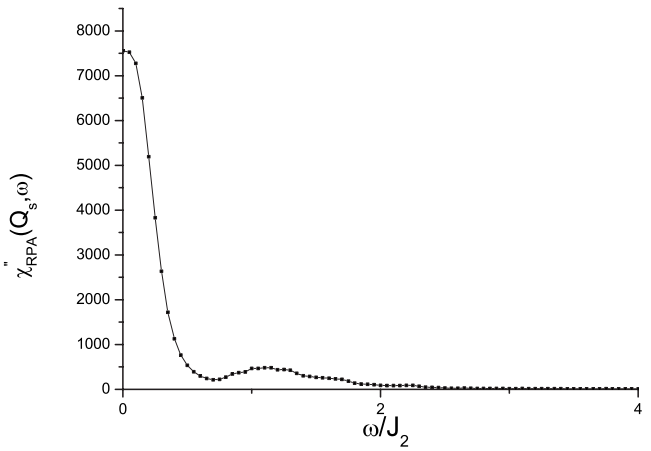

FIG. 7. Total dynamic spin susceptibility of coupled system in RPA level $\chi''_{\mathrm{RPA}}(\mathbf{q},\omega)$ fixing $\mathbf{q}=\mathbf{Q}_s$.

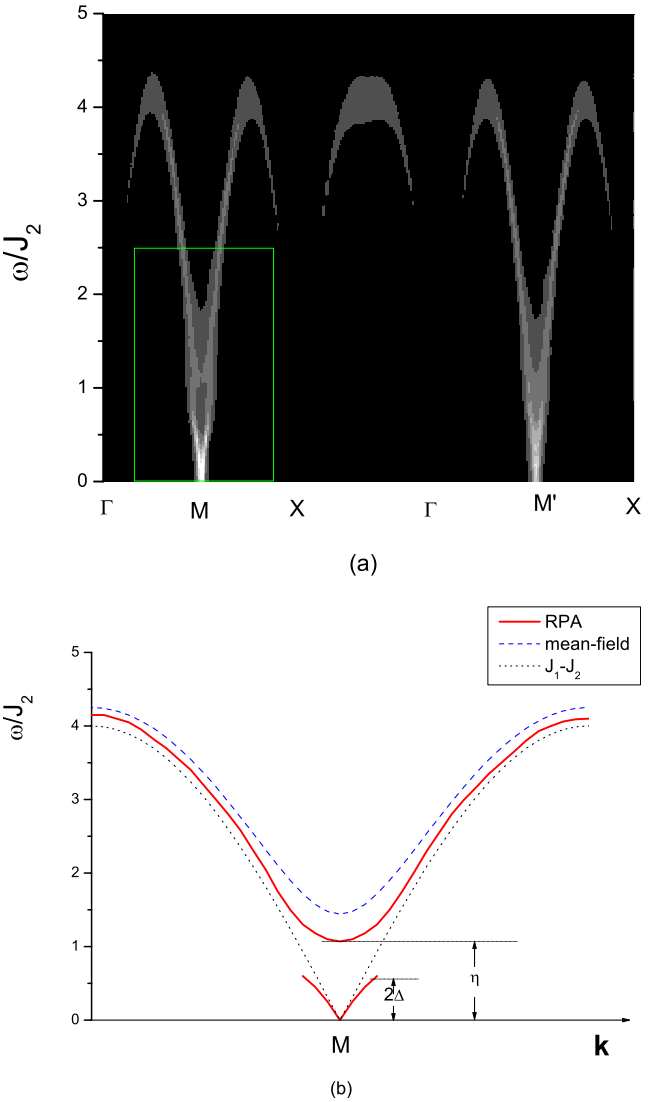

FIG. 8. (Color online) (a) The brightness represents the spectral weight of the dynamic spin susceptibility χ''_{RPA} in the $\mathbf{q}$ and ω space. (b) The dispersions of two branches of the collective spin mode as read from (a). The dispersions of the spin wave of the pure J_1-J_2 model (dotted) and that with a gap opening at the mean-field level (dashed) are also shown for comparison.

pling to the SDW order of the itinerant electrons are also shown for comparison.

The lower branch Goldstone mode in Fig. 8(b) is well defined within a small region which centers at the AF wave vector $\mathbf{Q}_s$, upper bounded by the SDW gap, i.e., $2\Delta_{\mathrm{SDW}}$ of the itinerant electrons, beyond which it decays quickly due to the scattering with the particle-hole continuum of itinerant electrons (cf. Fig. 4). Inside the SDW order gap, such a Goldstone mode is protected and is decoupled from the itinerant electrons due to the reconstruction of the Fermi surface shown in Figs. 1 and 2.

On the other hand, the high-energy out-of-phase mode is mainly contributed by the local moments and present throughout the BZ. It gets slight renormalization and broadening due to the scattering from the itinerant electrons at the

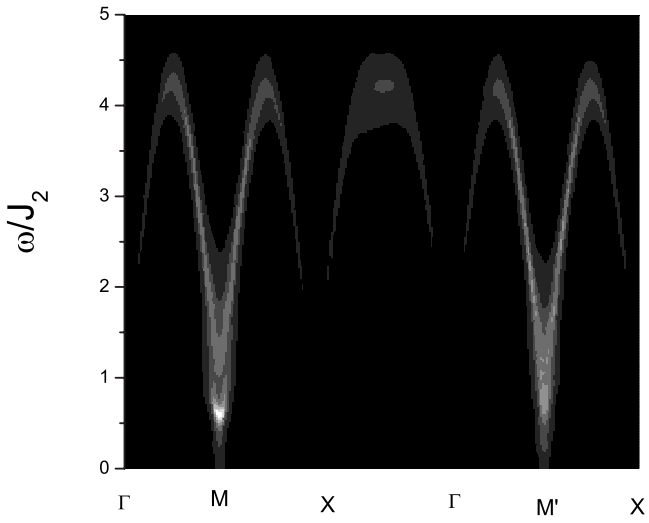

FIG. 9. The dynamic spin susceptibility similar to Fig. 8 but with an additional ion anisotropy $J_z=1$ meV.

RPA level, but more or less follows the dispersion obtained in the mean-field treatment (dotted), with a gap η,

$$\eta \approx \omega_{\mathbf{Q}_s}. \tag{43}$$

It is noted that the Goldstone mode will be fragile against the ion anisotropy. By adding an ion-anisotropy term,

$$H_{(\mathrm{ion})} = -J_z \sum_i (S_i^z)^2, \tag{44}$$

the spin-rotational symmetry will be broken in H_{lo}. By using the spin-wave expansion,

$$H_{(\mathrm{ion})} = 2SJ_z \sum_k{}' (a_{\mathbf{k}}^\dagger a_{\mathbf{k}} + b_{\mathbf{k}}^\dagger b_{\mathbf{k}}) + \mathrm{const} \tag{45}$$

one finds the spin-excitation spectrum, Eq. (16), acquires an ion-anisotropy gap,

$$\omega_{\mathbf{k}} = S\sqrt{(\Gamma_{\mathbf{k}} + 2J_z)^2 - M_{\mathbf{k}}^2}. \tag{46}$$

At the RPA level, the Goldstone spin wave will also become gapped and its spectrum weight is reduced with reference to that without ion anisotropy, as clearly shown in Fig. 9. When one further increases J_z, the Goldstone mode disappears, but the gapped out-of-phase collective mode remains robust and insensitive to the ion anisotropy.

Therefore, in the present coupled local moment and itinerant electron system, the Goldstone theorem still holds for a spontaneously symmetry breaking state with AF ordering at the RPA level. However, the Goldstone mode is very sensitive to the presence of ion anisotropy and does not play an important role for charge dynamics as it is decoupled from the itinerant electrons. On the other hand, the gapped out-of-phase collective mode is more prominent which extends over the whole BZ with a spin-wave bandwidth $\sim 4J_2$ and can be easily probed by neutron-scattering experiments. Such two-branch collective spin excitations are unique prediction for the AF ordered phase. In the next section, the charge response will be further examined based on the scattering of

such collective spin modes with the itinerant electrons in SDW ordering.

IV. CHARGE DYNAMICS

In this section, we study the charge dynamics in the coupled local-moment and itinerant-electron system in the AF ordered phase. Here the itinerant electrons in the Fermi-surface region will be highly coherent even in the presence of the gapless Goldstone mode.

A. Self-energy of itinerant electrons

By going beyond the mean-field linearization in Eq. (5), we shall consider the scattering based on

$$H_{J_H} \to H_I' = -\frac{J_0}{2\sqrt{N}} \sum_{\mathbf{k}\in R,\mathbf{q}\in R,\alpha\beta} c^\dagger_{\mathbf{k}\alpha\downarrow} c_{\mathbf{q}\beta\uparrow} [S^+_{\mathbf{q}-\mathbf{k}} V^{(1)}_{\mathbf{k},\mathbf{q}}(\alpha,\beta) + S^+_{\mathbf{q}-\mathbf{k}+\mathbf{Q}_s} V^{(2)}_{\mathbf{k},\mathbf{q}}(\alpha,\beta)] + \text{H.c.}$$
$$\equiv -\frac{J_0}{2\sqrt{N}} \sum_{\mathbf{k}\in R,\mathbf{q}\in R,\alpha\beta} c^\dagger_{\mathbf{k}\alpha\downarrow} c_{\mathbf{q}\beta\uparrow} R^+_{\mathbf{kq}\alpha\beta} + \text{H.c.}, \tag{47}$$

where the $V^{(1,2)}_{\mathbf{k},\mathbf{q}}(\alpha,\beta)$ are defined by Eq. (32). Here we retain only the scattering of itinerant electrons with the transverse fluctuations of local moments as the longitudinal fluctuations in S^z are gapped with $\langle S^z\rangle \neq 0$.

The single-particle Green's function can be evaluated perturbatively by

$$G_{\alpha\beta\downarrow}(\mathbf{k},\omega) = G^0_{\alpha\beta\downarrow}(\mathbf{k},\omega) + \sum_{\gamma\epsilon} G^0_{\alpha\gamma\downarrow}(\mathbf{k},\omega)\Sigma_{\gamma\epsilon\downarrow}(\mathbf{k},\omega)G^0_{\epsilon\beta\downarrow}(\mathbf{k},\omega) + O(H_I'^4), \tag{48}$$

where the self-energy,

$$\Sigma_{\gamma\epsilon\downarrow}(\mathbf{k},\omega) = \frac{iJ_0^2}{4N_{\mathbf{q}}} \sum_{\mathbf{q}\in R,\theta\xi} \int_{-\infty}^{+\infty} \frac{d\Omega}{2\pi} G^0_{\theta\xi\uparrow}(\mathbf{q},\omega-\Omega)\chi^{+-}_{(R)\mathbf{kq}\gamma\theta\xi\epsilon}(\Omega) \tag{49}$$

with

$$\chi^{+-}_{(R)\mathbf{kq}\gamma\theta\xi\epsilon}(\Omega) = \hat{\chi}^{+-}_{(\text{lo})(1,1)}(\mathbf{q}-\mathbf{k},\Omega)|V^{(1)}|^2 + \hat{\chi}^{+-}_{(\text{lo})(1,2)}(\mathbf{q}-\mathbf{k},\Omega)V^{(1)}V^{(2)*} + \hat{\chi}^{+-}_{(\text{lo})(2,1)}(\mathbf{q}-\mathbf{k},\Omega)V^{(2)}V^{(1)*} + \hat{\chi}^{+-}_{(\text{lo})(2,2)}(\mathbf{q}-\mathbf{k},\Omega)|V^{(2)}|^2. \tag{50}$$

Here the matrix $\hat{\chi}^{+-}_{(\text{lo})}$ is the dynamic spin correlation function for the local moment in the RPA level defined in Eq. (40). Figures 10 and 11 show the corresponding Feynman diagrams of the self-energy correction for itinerant electrons.

The Eq. (48) can be further expressed in a 10×10 matrix formalism by

$$G_{\mathbf{k},\omega} = G^0_{\mathbf{k},\omega} + G^0_{\mathbf{k},\omega}\Sigma_{\mathbf{k},\omega}G^0_{\mathbf{k},\omega} + \cdots = G^0_{\mathbf{k},\omega} + G^0_{\mathbf{k},\omega}\Sigma_{\mathbf{k},\omega}G_{\mathbf{k},\omega}, \tag{51}$$

which gives rise to $G_{\mathbf{k},\omega}=[(G^0_{\mathbf{k},\omega})^{-1}-(\Sigma_{\mathbf{k},\omega})]^{-1}$. Here we have omitted the spin index as they are in fact spin independent.

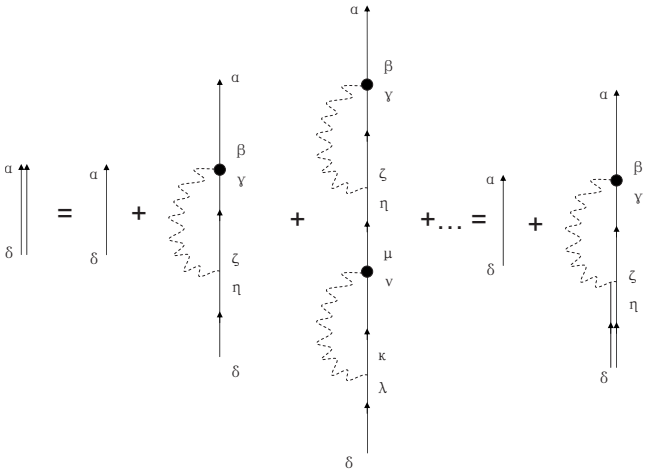

FIG. 10. Feynman diagrams of self-energy correction for itinerant electrons. Here the single black lines denote the propagators of (free) itinerant electrons, $G^0_{\alpha\delta}(\mathbf{k},\omega)$, the double black lines are the renormalized propagators of itinerant electrons, $G_{\alpha\delta}(\mathbf{k},\omega)$, the dotted wavy lines are the modified dynamic spin correlation of local moments in the RPA level $\chi^{+-}_{(R)\mathbf{kq}\gamma\theta\xi\epsilon}(\Omega)$ defined by Eq. (50). The indices α, β, γ, ρ, and ς, label different bands.

By noting that the zeroth-order single-particle Green's function is diagonal, through the Lehmann representation we have for $\omega>0$,

$$-\text{Im}\,\Sigma_{\gamma\epsilon}(\mathbf{k},\omega) = \frac{J_0^2}{4N}\sum_{\mathbf{q}\in R,\theta}\int_{-\infty}^{+\infty}\frac{d\Omega}{4\pi}\rho^0_\theta(\mathbf{q},\omega-\Omega) \times D^{+-}_{\gamma\theta\epsilon}(\mathbf{k}-\mathbf{q},\Omega)[n_B(\Omega)+n_F(\Omega-\omega)], \tag{52}$$

where

$$\rho^0_\theta(\mathbf{q},\omega) \equiv -2\,\text{Im}\,G^0_{\theta\theta}(\mathbf{q},\omega) \tag{53}$$

and

$$D^{+-}_{\gamma\theta\epsilon}(\mathbf{k}-\mathbf{q},\Omega) \equiv -2\,\text{Im}\,\chi^{+-}_{(R)\mathbf{kq}\gamma\theta\theta\epsilon}(\Omega) \tag{54}$$

are the spectral functions of single-particle and the modified dynamic spin susceptibility of the local moment, respectively.

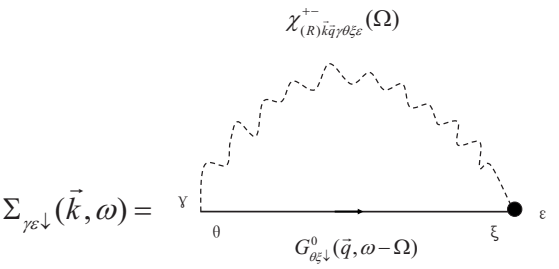

FIG. 11. Self-energy correction for itinerant electrons.

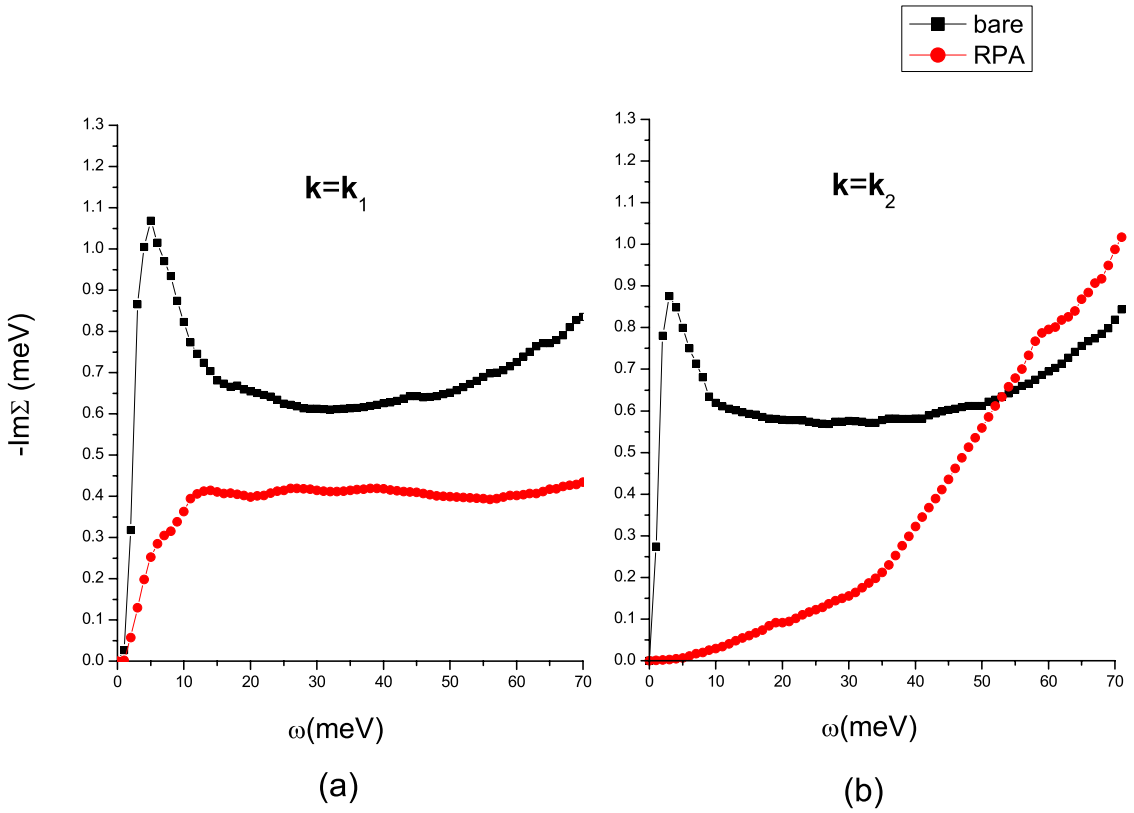

FIG. 12. (Color online) The imaginary part of the quasiparticle self-energy $-\mathrm{Im}\,\Sigma_{\alpha\alpha}(\mathbf{k},\omega)$ at two typical k points marked in Fig. 2(a) is shown. The red-circled curve is for incorporating the scattering with the full collective mode at the RPA level and the black-squared one is for the scattering with the bare local-moment fluctuations governed by H_{lo}.

At zero temperature, the imaginary self-energy, Eq. (52), can be further evaluated as (for $\omega>0$)

$$-\mathrm{Im}\,\Sigma_{\alpha\beta}(\mathbf{k},\omega)=\frac{J_0^2}{8N}\sum_{\mathbf{q}\in R,\theta,0<E_{\mathbf{q}\theta}<\omega}D^{+-}_{\alpha\theta\beta}(\mathbf{k}-\mathbf{q},\omega-E_{\mathbf{q}\beta}). \tag{55}$$

In Fig. 12, the $-\mathrm{Im}\,\Sigma_{\alpha\alpha}(\mathbf{k},\omega)$ as a function of ω is shown at two typical momenta, $(\mathbf{k}_1,\alpha_1)$ and $(\mathbf{k}_2,\alpha_2)$, respectively, which are marked at Fermi pockets in Fig. 2(a). It shows that the lifetime of the quasiparticle excitations at these points of Fermi pockets actually gets substantially *enhanced* at low ω in the collinear AF ordered state (solid circles), as compared to an artificial case (solid squares) without an induced SDW order appearing in itinerant electrons such that there is no gap η opened up in the out-of-phase mode. It implies that although in the normal state the itinerant electrons may be strongly scattered by the low-lying local moment fluctuations, the sharp coherence of quasiparticles will emerge in the AF state, where the gapless Goldstone mode is essentially decoupled from the particle-hole continuum and the out-of-phase mode is gapped.

B. Optical conductivity

Finally, let us examine the overall structure of the optical conductivity $\sigma(\omega)$ at the mean-field and RPA levels. It is related to the current-current correlation function $G_J(\omega)$ through the relation

$$\sigma(\omega)=-\frac{1}{\omega}\mathrm{Im}\,G_J(\omega), \tag{56}$$

where $G_J(\omega)$ is the Fourier transformation of the current-current correlator

$$G_J(t)\equiv -i\langle TJ(t)J(0)\rangle. \tag{57}$$

Here J denotes the $\mathbf{q}=0$ current operator $\mathbf{J}$ along, say, the x axis for the five-band model, Eq. (2), defined by

$$\begin{aligned}\mathbf{J}&=\left.\frac{\partial H_{it}(\mathbf{A})}{\partial\mathbf{A}}\right|_{\mathbf{A}=0}=\sum_{\mathbf{k}\sigma mn}\vec{\nabla}_{\mathbf{k}}f_{mn}(\mathbf{k})c^{+}_{\mathbf{k}m\sigma}c_{\mathbf{k}n\sigma}\\&=\sum_{\mathbf{k}\in R,\sigma mn\alpha\beta}c^{\dagger}_{\mathbf{k}\alpha\sigma}c_{\mathbf{k}\beta\sigma}[\vec{\nabla}_{\mathbf{k}}f_{mn}(\mathbf{k})U^{*}_{\mathbf{k}\sigma}(m,\alpha)U_{\mathbf{k}\sigma}(n,\beta)\\&\quad+\vec{\nabla}_{\mathbf{k}}f_{mn}(\mathbf{k}+\mathbf{Q}_s)U^{*}_{\mathbf{k}\sigma}(m+5,\alpha)U_{\mathbf{k}\sigma}(n+5,\beta)]\\&\equiv\sum_{\mathbf{k}\in R,\sigma\alpha\beta}V_{\mathbf{k}\sigma\alpha\beta}c^{\dagger}_{\mathbf{k}\alpha\sigma}c_{\mathbf{k}\beta\sigma}.\end{aligned} \tag{58}$$

Omitting the vertex correction, we find

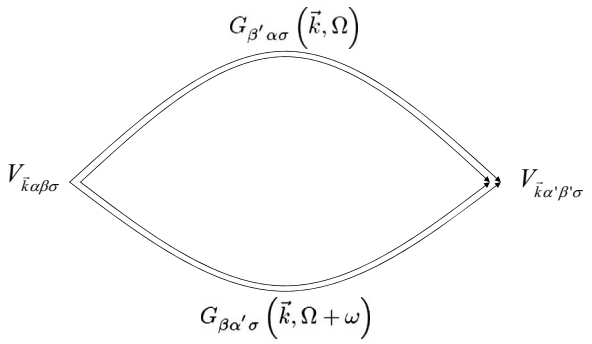

FIG. 13. Current-current correlation function for itinerant electrons. Here the double black lines are the renormalized propagators of itinerant electrons.

$$G_J(\omega) = -\frac{i}{N}\sum_{\mathbf{k}\in R,\sigma,\alpha\beta,\alpha'\beta'}\int_{-\infty}^{+\infty}\frac{d\Omega}{2\pi}V_{\mathbf{k}\sigma\alpha\beta}V_{\mathbf{k}\sigma\alpha'\beta'} \times G_{\beta'\alpha\sigma}(\mathbf{k},\Omega)G_{\beta\alpha'\sigma}(\mathbf{k},\Omega+\omega) \quad (59)$$

with the Feynman diagrams shown in Fig. 13. Denoting

$$\rho_{\alpha\beta}(\mathbf{k},\omega) \equiv -2\ \mathrm{Im}\ G_{\alpha\beta\sigma}(\mathbf{k},\omega)\mathrm{sgn}(\omega) \quad (60)$$

at $T=0$ we obtain

$$-\mathrm{Im}\ G_J = \frac{1}{N}\sum_{\mathbf{k}\in R,\sigma,\alpha\beta,\alpha'\beta'}\int_{-\omega}^{0}\frac{d\Omega}{2\pi}V_{\mathbf{k}\sigma\alpha\beta}V_{\mathbf{k}\sigma\alpha'\beta'} \times \rho_{\beta'\alpha}(\mathbf{k},\Omega)\rho_{\beta\alpha'}(\mathbf{k},\Omega+\omega) \quad (61)$$

such that

$$\sigma(\omega) = \frac{1}{N\omega}\sum_{\mathbf{k}\in R,\sigma,\alpha\beta,\alpha'\beta'}\int_{-\omega}^{0}\frac{d\Omega}{2\pi}V_{\mathbf{k}\sigma\alpha\beta}V_{\mathbf{k}\sigma\alpha'\beta'} \times \rho_{\beta'\alpha}(\mathbf{k},\Omega)\rho_{\beta\alpha'}(\mathbf{k},\Omega+\omega). \quad (62)$$

The calculated optical conductivity $\sigma(\omega)$ is shown in Fig. 14. The black-squared curve shows the result for the bare five-band itinerant electrons and the red circles represent the result of the SDW reconstructed bands. Note that the multipeak structure is mainly due to the multiband effect with the lower ones changing significantly in the SDW state. Furthermore, by incorporating the scattering with the collective spin modes at the RPA level, as shown by the blue triangles in Fig. 14, no significant change has been found in the optical conductivity with $\mathbf{q}=0$. It clearly illustrated that the itinerant electrons remain very coherent in the AF ordered phase, where the low-lying Goldstone mode does not strongly scatter the quasiparticles as expected.

V. DISCUSSION AND CONCLUSION

In this work, we have studied the collective spin excitations in the AF ordered phase of a multicomponent system composed of coexistent itinerant and localized electrons. The main prediction is that a usual spin mode is split into two branches in such a multiband system with orbital-selective Mott transition. The lower branch is a gapless Goldstone

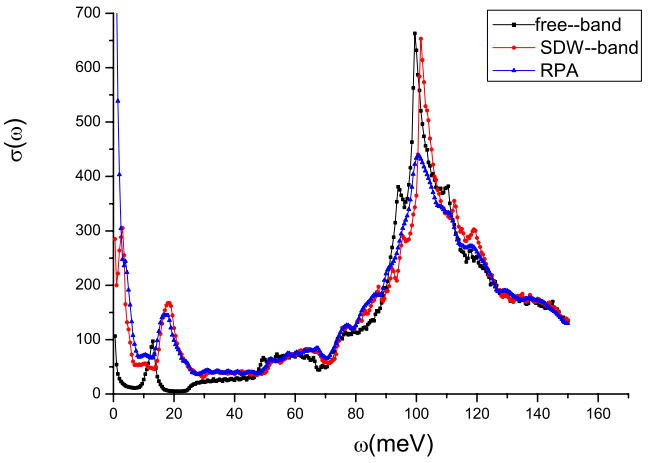

FIG. 14. (Color online) The optical conductivity $\sigma(\omega)$ in the AF ordered state (blue solid triangle) which shows that the quasiparticles remain quite coherent as compared to the case without incorporating the scattering with the collective spin modes (red solid circles). For comparison, $\sigma(\omega)$ for the pure five-band model without the SDW reconstruction is shown (black square).

mode which is recovered at the RPA level and is quickly damped above $2\Delta_{\mathrm{SDW}}$ by coupling to the particle-hole continuum of itinerant electrons, similar to the case in which the SDW order is due to the pure Fermi-surface nesting effect for itinerant electrons. However, an upper branch remnant spin wave reemerges above the SDW gap over a much wider energy $\sim J_2$ which is dominantly contributed by the local moment fluctuations. Here the lower and upper branches can be regarded as in-phase and out-of-phase combinations of the spin fluctuations from the itinerant and Mott-localized electrons, which are clearly distinguished from the single mode in a conventional AF state either due to the pure Fermi-surface nesting effect for itinerant electrons or AF superexchanges of local moments.

Experimentally the high-energy spin-wave excitation has been clearly observed by the neutron-scattering experiments over an energy scale $\sim J_2$ and presumably survives in the high-temperature regime above the ordered phase. However, a small gap ($\sim$6–10 meV) has been generally found in $SrFe_2As_2$ and $BaFe_2As_2$, and interpreted as due to ion anisotropy.[33,34] As shown in this work, a small ion anisotropy can indeed easily destroy the lower branch Goldstone mode, while the upper branch is more robust. It remains to be seen if the lower branch spin mode can be unambiguously identified for a sample with less ion anisotropy.

Another distinct property of the present system is that the itinerant electrons become very coherent in the AF ordered phase, leading to a good metallic behavior after the AF transition. This is in contrast to the presumably strong scattering between the itinerant electrons and local moments in the normal state, where due to the very fact that the momentum displacement of the hole-electron Fermi pockets of the itinerant electrons matches with the AF wave vector of the local moments, there exists a strongly enhanced interaction, i.e., the *resonant effect* around $\mathbf{Q}_s$, between the two subsystems. It provides the strong scattering source responsible for a drastic change in the charge response once the system enters

the AF long-range ordered state at low temperature. By forming a joint magnetic ordering, the two subsystem effectively get "decoupled" as the AF fluctuations of the local moments gain a gap η as the out-of-phase collective mode. On the other hand, the gapless Goldstone mode is effectively decoupled from the itinerant electrons in the long wavelength, thanks to the Fermi-surface reconstruction by the SDW order.

Therefore, the collective fluctuations of the local moments can serve as the main driving force for both the AF ordering as well as the superconducting pairing in the system via the resonant effect on itinerant electrons, as first pointed out in Ref. 30. The resulting magnetic and charge properties in the AF ordered state, in particular, the two branch collective spin modes predicted in the present work, can be further tested by experiment in order to establish the relevance of the model with the iron pnictides.

ACKNOWLEDGMENTS

We acknowledge stimulating discussions with X. H. Chen, P. C. Dai, D. L. Feng, D. H. Lee, P. A. Lee, T. Li, Z. Y. Lu, N. L. Wang, T. Xiang, Y. Z. You, G. M. Zhang, and H. Yao. The authors are grateful for the partial support by NSFC under Grant Nos. 10688401, 10704008, 10834003, and 10874017 as well as the National Program for Basic Research of MOST.

*weng@tsinghua.edu.cn

[1] Y. Kamihara, T. Watanabe, M. Hirano, and H. Hosono, J. Am. Chem. Soc. **130**, 3296 (2008).
[2] P. W. Anderson, Science **235**, 1196 (1987).
[3] J. Dong, H. J. Zhang, G. Xu, Z. Li, G. Li, W. Z. Hu, D. Wu, G. F. Chen, X. Dai, J. L. Luo, Z. Fang, and N. L. Wang, EPL **83**, 27006 (2008).
[4] C. Cao, P. J. Hirschfeld, and H. P. Cheng, Phys. Rev. B **77**, 220506(R) (2008).
[5] D. J. Singh and M. H. Du, Phys. Rev. Lett. **100**, 237003 (2008).
[6] I. I. Mazin, D. J. Singh, M. D. Johannes, and M. H. Du, Phys. Rev. Lett. **101**, 057003 (2008).
[7] K. Kuroki, S. Onari, R. Arita, H. Usui, Y. Tanaka, H. Kontani, and H. Aoki, Phys. Rev. Lett. **101**, 087004 (2008).
[8] C. de la Cruz, Q. Huang, J. W. Lynn, J. Li, W. Ratcliff II, J. L. Zarestky, H. A. Mook, G. F. Chen, J. L. Luo, N. L. Wang, and P. Dai, Nature (London) **453**, 899 (2008).
[9] D. H. Lu, M. Yi, S. K. Mo, A. S. Erickson, J. Analytis, J. H. Chu, D. J. Singh, Z. Hussain, T. H. Geballe, I. R. Fisher, and Z. X. Shen, Nature (London) **455**, 81 (2008).
[10] G. Liu, H. Liu, L. Zhao, W. Zhang, X. Jia, J. Meng, X. Dong, J. Zhang, G. F. Chen, G. Wang, Y. Zhou, Y. Zhu, X. Wang, Z. Xu, C. Chen, and X. J. Zhou, Phys. Rev. B **80**, 134519 (2009).
[11] L. X. Yang, Y. Zhang, H. W. Ou, J. F. Zhao, D. W. Shen, B. Zhou, J. Wei, F. Chen, M. Xu, C. He, Y. Chen, Z. D. Wang, X. F. Wang, T. Wu, G. Wu, X. H. Chen, M. Arita, K. Shimada, M. Taniguchi, Z. Y. Lu, T. Xiang, and D. L. Feng, Phys. Rev. Lett. **102**, 107002 (2009).
[12] M. Tropeano *et al.*, Supercond. Sci. Technol. **22**, 034004 (2009).
[13] W. Z. Hu, J. Dong, G. Li, Z. Li, P. Zheng, G. F. Chen, J. L. Luo, and N. L. Wang, Phys. Rev. Lett. **101**, 257005 (2008).
[14] T. Yildirim, Phys. Rev. Lett. **101**, 057010 (2008).
[15] Q. Si and E. Abrahams, Phys. Rev. Lett. **101**, 076401 (2008).
[16] F. Ma, Z. Y. Lu, and T. Xiang, Phys. Rev. B **78**, 224517 (2008).
[17] J. Zhao, D. T. Adroja, D. X. Yao, R. Bewley, S. Li, X. F. Wang, G. Wu, X. H. Chen, J. P. Hu, and P. C. Dai, Nat. Phys. **5**, 555 (2009).
[18] M. J. Han, Q. Yin, W. E. Pickett, and S. Y. Savrasov, Phys. Rev. Lett. **102**, 107003 (2009).
[19] I. I. Mazin, M. D. Johannes, L. Boeri, K. Koepernik, and D. J. Singh, Phys. Rev. B **78**, 085104 (2008).
[20] M. D. Johannes, I. I. Mazin, Phys. Rev. B **79**, 220510(R) (2009).
[21] H. S. Jeevan, Z. Hossain, D. Kasinathan, H. Rosner, C. Geibel, and P. Gegenwart, Phys. Rev. B **78**, 052502 (2008).
[22] R. Arita and H. Ikeda, J. Phys. Soc. Jpn. **78**, 113707 (2009).
[23] X. F. Wang, T. Wu, G. Wu, H. Chen, Y. L. Xie, J. J. Ying, Y. J. Yan, R. H. Liu, and X. H. Chen, Phys. Rev. Lett. **102**, 117005 (2009).
[24] R. Klingeler, N. Leps, I. Hellmann, A. Popa, U. Stockert, C. Hess, V. Kataev, H. J. Grafe, F. Hammerath, G. Lang, S. Wurmehl, G. Behr, L. Harnagea, S. Singh, and B. Buchner, Phys. Rev. B **81**, 024506 (2010).
[25] G. M. Zhang, Y. H. Su, Z. Y. Lu, Z. Y. Weng, D. H. Lee, and T. Xiang, EPL **86**, 37006 (2009).
[26] X. H. Chen, T. Wu, G. Wu, R. H. Liu, H. Chen, and D. F. Fang, Nature (London) **453**, 761 (2008).
[27] Y. Luo, Y. Li, S. Jiang, J. Dai, G. Cao, and Z. Xu, Phys. Rev. B **81**, 134422 (2010).
[28] T. Sato, K. Nakayama, Y. Sekiba, P. Richard, Y.-M. Xu, S. Souma, T. Takahashi, G. F. Chen, J. L. Luo, N. L. Wang, and H. Ding, Phys. Rev. Lett. **103**, 047002 (2009).
[29] C. Liu, G. D. Samolyuk, Y. Lee, N. Ni, T. Kondo, A. F. Santander-Syro, S. L. Bud'ko, J. L. McChesney, E. Rotenberg, T. Valla, A. V. Fedorov, P. C. Canfield, B. N. Harmon, and A. Kaminski, Phys. Rev. Lett. **101**, 177005 (2008).
[30] S. P. Kou, T. Li, and Z. Y. Weng, EPL **88**, 17010 (2009).
[31] L. de' Medici, S. R. Hassan, and M. Capone, J. Supercond. Novel Magn. **22**, 535 (2009).
[32] H. Lee, Y. Zhang, H. Jeschke, and R. Valenti, Phys. Rev. B **81**, 220506 (2010).
[33] J. Zhao, D.-X. Yao, S. Li, T. Hong, Y. Chen, S. Chang, W. Ratcliff, J. W. Lynn, H. A. Mook, G. F. Chen, J. L. Luo, N. L. Wang, E. W. Carlson, J. Hu, and P. Dai, Phys. Rev. Lett. **101**, 167203 (2008).
[34] K. Matan, R. Morinaga, K. Iida, and T. J. Sato, Phys. Rev. B **79**, 054526 (2009).